Interstitial-electron model for lattice dynamics in fcc metals

Mo Li and William A. Goddard III
Arthur Amos Noyes Laboratory of Chemical Physics, California Institute of Technology, Pasadena, California 91125
(Received 24 July 1989; revised manuscript received 21 November 1989)

We propose and test the interstitial-electron model (IEM) for lattice dynamics in close-packed structures. The IEM model treats the valence electrons as classical lattice particles localized at interstitial tetrahedral positions, as suggested by the *ab initio* generalized-valence-bond cluster calculations of McAdon and Goddard. We apply the IEM to the fcc metals Ni, Pd, Pt, Ag, Au, and Cu using a simple six-parameter description (nearest-neighbor electron-electron, electron-ion, ion-ion terms, each with two parameters) to exactly fit lattice constants, elastic constants (C_{11}, C_{12}, C_{44}), and the two lattice modes at the X point in the first Brillouin zone. The predicted phonon-dispersion relations are in excellent agreement with experiment for all branches in the high-symmetry [100], [110], and [111] directions. The explicit inclusion of valence electrons in the interparticle interactions implicitly includes what would be considered as many-body effects in the usual ion-ion scheme (e.g., $C_{12} \neq C_{44}$). Such force fields should also be useful for describing nonperiodic systems (surfaces, clusters, and defects).

I. INTRODUCTION

Recent *ab initio* quantum-mechanical calculations by McAdon and Goddard[1,2] of many-body electron-correlation effects in small metal clusters (6–14 atoms) showed that the electrons tend to localize into interstitial regions with each electron in a different site. This is illustrated in Fig. 1 for the icosahedral cluster of Li_{13}^{+}, where the 12 electrons each localize in a different tetrahedron. In the ground state, pairs of such interstitial orbitals are singlet paired but the states with triplet and higher pairing are low-lying excited states. In contrast, similar calculations on nonmetallic clusters (e.g., C, Si, etc.) lead to two-electron bonds, each localized between two atoms. In this case, the two generalized-valence-bond (GVB) orbitals are singlet paired and localize along the bond with one orbital toward each atom. Triplet pairing of these orbitals leads to high-lying antibonding excited states. The major factor distinguishing the metallic and nonmetallic clusters is that the metallic clusters have far more bonding orbitals than electrons so that it is possible to account for all electrons by singly occupying orbitals that are in different bond regions. McAdon and Goddard suggested that this description in terms of interstitial electrons would apply to infinite fcc metals (quantum-mechanical GVB calculations are not yet possible on such systems) and suggested that two- and three-body potentials incorporating the valence electrons explicitly might be useful.

Based on the GVB calculations, we propose and test the interstitial electron model (IEM) for face-centered cubic metals. In this model we consider that an electron can localize at each of the tetrahedral locations in a fcc metal (two sites per atom). At equilibrium, each orbital is centered in the tetrahedral site, but the orbital would shift position adiabatically under lattice vibrations. With IEM we treat the various electrons as pseudoparticles of a small mass (zero in the current calculations) whose center corresponds to the center of the GVB orbital. The quantum mechanics of the electronic states is replaced by potentials depending upon the electron-ion and electron-electron distances. As a first test of this model we simpli-

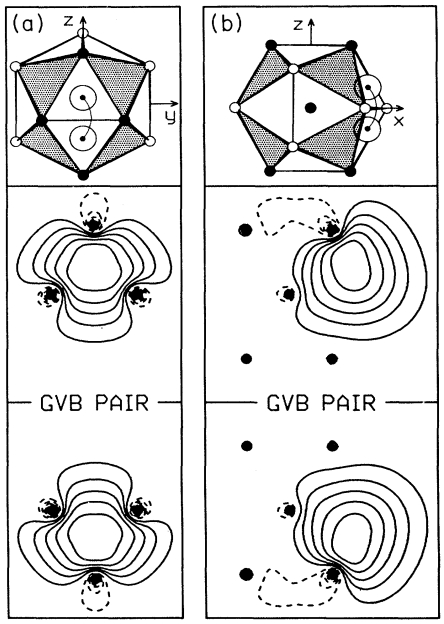

FIG. 1. GVB orbitals for the icosahedral Li_{13}^{+} cluster. Each orbital is in a different tetrahedron and spin paired to an orbital in an adjacent tetrahedron (from Ref. 1). Shown are two views, (a) a top view and (b) side view, of the two GVB orbitals of one pair localized in the two tetrahedral along the $+x$ axis. There are equivalent pairs along the $-x$, $\pm y$, and $\pm z$ directions. In each case the atoms in the plotting plane are marked by solid circles, while atoms above and below the plane are marked by open circles. Connected dots represent the spin-paired electrons. Shaded triangular faces do not contain orbitals. Overlaps of spin-paired orbitals are 0.63.

 ©1989 The American Physical Society

fy the IEM to include only pairwise interactions of nearest neighbors, with three independent potentials:

(i) $\phi_{i\text{-}i}(\mathbf{r})$ for ion-ion interactions ,

(ii) $\phi_{i\text{-}e}(\mathbf{r})$ for ion-electron interactions ,

(iii) $\phi_{e\text{-}e}(\mathbf{r})$ for electron-electron interactions , (1)

and where just two parameters ($\phi'=d\phi/dr$ and $\phi''=d^2\phi/dr^2$ evaluated at the nearest-neighbor distance) are used for each two-body potential. These restrictions are made solely to simplify these initial studies. It is plausible that longer-range interactions and three-body terms (e.g., ion-electron-ion, electron-ion-electron, etc.) should be present, but they are not included here.

In this paper we test the efficacy of this description by using the IEM to fit the lattice dynamics and elastic constants of six fcc metals: Ni, Pd, Pt, Cu, Ag, and Au. Thus we approximate each electron as a classical lattice particle centered at each tetrahedral interstitial site and treat the electron and the ions equally in setting up the dynamical matrix. We find that this approach (using only nearest-neighbor interactions with a total of six adjustable parameters) leads to a description of the lattice dynamics in excellent agreement with experiment.

In Sec. II we present the general formalism of the IEM for describing lattice dynamics and for calculating the elastic constants. The numerical results and comparisons with other first-principle and phenomenological models are illustrated in Sec. III. Section IV includes some analysis of the results including a comparison with this method and some ideas on extending the IEM to simulations of more complicated systems.

II. MODEL

Within the harmonic approximation, the equations of motion for the lattice particles become

$$M_k\omega^2(\mathbf{q})u_\alpha(k)=\sum_{k',\beta} D_{\alpha\beta}\begin{bmatrix}\mathbf{q}\\ k k'\end{bmatrix}u_\beta(k') \tag{2}$$

where k denotes each lattice particle (electron *and* nucleus) in the unit cell, $u_\alpha(k)$ are the normal mode coordinates for energy (ω) and wave vector ($\mathbf{q}$), and M_k is the mass. The components of the dynamical matrix are given by

$$D_{\alpha\beta}\begin{bmatrix}\mathbf{q}\\ k k'\end{bmatrix}=\sum_{l'}\Phi_{\alpha\beta}\begin{bmatrix}l & l'\\ k & k'\end{bmatrix}\exp\left[-i\mathbf{q}\cdot\mathbf{r}\begin{bmatrix}l & l'\\ k & k'\end{bmatrix}\right] \tag{3}$$

where (a) $\mathbf{r}\binom{l}{k}$ is the position of the kth lattice particle in the lth cell, (b) $x_\alpha\binom{l}{k}$ is its Cartesian component, (c) α,β are the Cartesian indices, and (d) the force constant matrix of the particles separated by $\mathbf{r}\binom{l\ l'}{k\ k'}=\mathbf{r}\binom{l}{k}-\mathbf{r}\binom{l'}{k'}$, or $\binom{l\ l'}{k\ k'}$, is given by

$$\Phi_{\alpha\beta}\begin{bmatrix}l & l'\\ k & k'\end{bmatrix}=-\frac{\partial^2\phi\binom{l\ l'}{k\ k'}}{\partial x_\alpha\binom{l}{k}\partial x_\beta\binom{l'}{k'}} . \tag{4}$$

For fcc metals the unit cell contains one ion and two interstitial electron particles at [000], $[\frac{1}{4}\frac{1}{4}\frac{1}{4}]$, and $[\frac{3}{4}\frac{3}{4}\frac{3}{4}]$, respectively.

In the current calculations we take the mass of the electron M_k to be zero (analogous to the Born-Oppenheimer approximation). A nonzero mass of the electrons would be used to describe plasma oscillations and the response of the electrons to high-frequency fields. Transforming to remove the electron coordinates reduces (2) to the equations of motion for the ions

$$M_k\omega^2(\mathbf{q})u_\alpha(k)=\sum_{k',\beta} D^{\text{tot}}_{\alpha\beta}\begin{bmatrix}\mathbf{q}\\ k k'\end{bmatrix}u_\beta(k') \tag{5}$$

where k,k' describes ions only. The components of the new dynamical matrix $D^{\text{tot}}_{\alpha\beta}$ are

$$D^{\text{tot}}_{\alpha\beta}\begin{bmatrix}\mathbf{q}\\ k k'\end{bmatrix}=D^{i\text{-}i}_{\alpha\beta}\begin{bmatrix}\mathbf{q}\\ k k'\end{bmatrix}-D^{i\text{-}e}_{\alpha\gamma}\begin{bmatrix}\mathbf{q}\\ k s\end{bmatrix}D^{e\text{-}e}_{\gamma\lambda}\begin{bmatrix}\mathbf{q}\\ s s'\end{bmatrix}^{-1}D^{e\text{-}i}_{\lambda\beta}\begin{bmatrix}\mathbf{q}\\ s' k'\end{bmatrix} \tag{6}$$

where s,s' denotes electrons. The summation convention is used here for repeated indices. Each type of dynamical matrix in (6) is still given by (3) and (4) but we use superscripts *i-i*, *i-e*, and *e-e* to emphasize the type of interaction. Thus we use $\phi\binom{l\ l'}{k\ k'}$ for ion-ion ($D^{i\text{-}i}$), $\phi\binom{l\ l}{k\ s}$ for ion-electron ($D^{i\text{-}e}$), and $\phi\binom{l\ l'}{s\ s'}$ for electron-electron ($D^{e\text{-}e}$). The dynamic matrices can be obtained from force constant matrices such as are given in the Appendix. The secular equation

$$\left|D^{\text{tot}}_{\alpha\beta}\begin{bmatrix}\mathbf{q}\\ k k'\end{bmatrix}-\delta_{\alpha\beta}\delta_{kk'}M_{k'}\omega^2(\mathbf{q})\right|=0 \tag{7}$$

gives the phonon-dispersion relations $\omega(\mathbf{q})$.

In order to keep the model simple, we limited the present calculations to first nearest neighbors for each of the three types of interactions in (1). Since only nearest-neighbor terms are included, a total of six parameters ($\phi'_{i\text{-}i}$, $\phi''_{i\text{-}i}$, $\phi'_{i\text{-}e}$, $\phi''_{i\text{-}e}$, $\phi'_{e\text{-}e}$, and $\phi''_{e\text{-}e}$) is used in (6) for the IEM (see Appendix). The symmetry group of the bonds for the first nearest neighbors reduces the components of the corresponding force constant matrix (which are linear superpositions of the above six parameters) to a total of seven, one of which is the linear superposition of the others. Instead of using the parameters ϕ' and ϕ'' directly, we employ six independent force constants (α, γ, μ, λ, δ, and ρ) as free parameters in the lattice dynamical calculations,

$$\begin{aligned}
\alpha&=-\frac{1}{a\sqrt{2}}\phi'_{i\text{-}i}-\tfrac{1}{2}\phi''_{i\text{-}i} ,\\
\gamma&=\frac{1}{a\sqrt{2}}\phi'_{i\text{-}i}-\tfrac{1}{2}\phi''_{i\text{-}i} ,\\
\mu&=-\frac{8}{a3\sqrt{3}}\phi'_{i\text{-}e}-\tfrac{1}{3}\phi''_{i\text{-}e} ,\\
\lambda&=\frac{4}{a3\sqrt{3}}\phi'_{i\text{-}e}-\tfrac{1}{3}\phi''_{i\text{-}e} ,\\
\delta&=-\phi''_{e\text{-}e} ,\\
\rho&=-\frac{2}{a}\phi'_{e\text{-}e} ,
\end{aligned} \tag{8}$$

where a is the cubic lattice constant.

The phonon-dispersion relations $\omega(\mathbf{q})$ in the three high-symmetry directions [100], [110], and [111] were ob-

tained by solving (7). The [100] branches are related to the force constants by

$$M_k\omega_L^2(\mathbf{q})=-16\alpha\sin^2\left[\frac{\pi}{2}q\right]-8\mu+\frac{8\mu^2\cos^2\left[\frac{\pi}{2}q\right]}{\mu+\delta\sin^2\left[\frac{\pi}{2}q\right]}\,,$$

$$M_k\omega_T^2(\mathbf{q})=-8(2\alpha-\gamma)\sin^2\left[\frac{\pi}{2}q\right]-8\mu+\frac{8\mu^2\cos^2\left[\frac{\pi}{2}q\right]}{\mu+\rho\sin^2\left[\frac{\pi}{2}q\right]}+\frac{8\lambda^2\sin^2\left[\frac{\pi}{2}q\right]}{\mu+\delta+\rho\left[1+\cos^2\left[\frac{\pi}{2}q\right]\right]}\,, \tag{9}$$

where q is the reduced wave vector, $q=|\mathbf{q}|/q_{\max}$. The $q_{\max}$ equals $2\pi/a$, $2\sqrt{2}\,\pi/a$, and $2\sqrt{3}\,\pi/a$ in the [100], [110], and [111] directions, respectively. The corresponding dispersion relations for the [111] and [110] branches are given in the Appendix. It is clear from (9) that the ion-electron (μ,λ) and electron-electron (δ,ρ) terms modify the $\omega(\mathbf{q})$ from that of the ion-ion interactions (α,γ). The electron contributions to the phonon-dispersion relations become substantial in all branches at large q, where the electrons vibrate out of phase with ions.

In the long-wave limit ($\mathbf{q}\to 0$) the equilibrium conditions and three elastic constants can be expressed in terms of the force constants,

$$-2\alpha+2\gamma-\mu+\lambda-\rho=0\,, \tag{10}$$

$$C_{11}=-\frac{a^2}{2V_a}(2\alpha+\mu+\delta)\,,$$

$$C_{12}=-\frac{a^2}{2V_a}(-2\alpha+3\gamma-\mu+2\lambda-\rho)\,,$$

$$C_{44}=-\frac{a^2}{2V_a}\left[2\alpha-\gamma+\mu+\rho-\frac{\lambda^2}{\mu+\delta+2\rho}\right]\,, \tag{11}$$

where $V_a=\frac{1}{4}a^3$ is the volume per atom.

Using only pairwise ion-ion interactions (where μ, λ, δ, and ρ are all zero) leads to the Cauchy relation $C_{12}=C_{44}$; whereas real metals lead to very different values ($C_{12}\approx 4C_{44}$ for Pt and Au). However, IEM leads to the Cauchy discrepancy of

$$C_{12}-C_{44}=-\frac{a^2}{2V_a}\frac{\lambda^2}{\mu+\delta+2\rho}\,, \tag{12}$$

and the optimum parameters agree exactly with experiment. Thus the many-body effects implicit in the μ, λ, δ, and ρ parameters of the ion-electron and electron-electron interactions lead to the correct nonzero values.[3]

III. NUMERICAL CALCULATIONS

The six free parameters introduced in the interstitial electron model were determined analytically by solving six equations: the equilibrium condition (10), the three elastic constants (11), and the two vibrational frequencies at the X point in the [100] direction,

$$M_k\omega_L^2(\mathbf{q}_X)=-16\alpha-8\mu \tag{13}$$

and

$$M_k\omega_T^2(\mathbf{q}_X)=-8(2\alpha-\gamma)-8\mu+\frac{8\lambda^2}{\mu+\delta+\rho}\,. \tag{14}$$

The lattice constant (a), elastic constants (C_{11}, C_{12}, C_{44}), and vibration frequencies $[\omega_L(\mathbf{q}_X),\omega_T(\mathbf{q}_X)]$ are taken from experiment (Refs. 4–10) and tabulated in Table I.

The parameters were determined by the above six equations, which ultimately lead to a cubic equation for ρ. In each case there are three real solutions leading to three different sets of parameters. Among those sets of parameters, two ultimately give imaginary phonon dispersion relations. Therefore, only one solution is acceptable, leading to a unique set of parameters. These parameters are given in Table II for Ni, Pd, Pt, Cu, Ag, and Au, while the ϕ' and ϕ'' from (8) are given in Table III. These parameters reproduce the quantities in Table I to the accuracy of the calculations (nine decimal values).

Using these parameters, we calculated the phonon-dispersion relations in the three high-symmetry directions (where data are available from experiment). We find excellent agreement with experiments, as shown in Figs. 2–7.

TABLE I. Experimental data used in fitting parameters to the IEM.

	Ni	Cu	Pd	Ag	Pt	Au
a (Å)	3.5239	3.6150	3.8907	4.0857	3.9239	4.0780
C_{11} (GPa)[a]	250.80	168.40	230.80	124.00	346.70	193.00
C_{12} (GPa)	150.00	121.40	176.20	93.40	250.70	163.44
C_{44} (GPa)	123.50	75.40	70.00	46.10	76.50	42.00
ω_X^L (THz)	8.550	7.190	6.720	4.936	5.780	4.610
ω_X^T (THz)	6.170	5.080	4.640	3.448	3.730	2.750
Mass (amu)	58.710	63.540	106.400	107.873	195.090	197.000

[a] 1 GPa $=10^{10}$ dyn/cm^2.

TABLE II. Theoretical parameters describing the IEM potentials. All quantities in units of erg/cm^2=dyn/cm.

	Ni	Cu	Pd	Ag	Pt	Au
α	−170.233	1676.728	7665.901	3993.953	7687.027	7306.492
γ	−11 288.606	−5093.518	−1267.643	−1586.597	895.448	1535.036
μ	−34 753.832	−30 212.914	−54 620.932	−29 478.840	−66 668.619	−48 847.195
λ	−15 140.644	−16 849.532	−33 009.424	−17 493.622	−50 081.534	−34 860.452
δ	−9095.409	−3578.843	−5069.548	−3840.405	−14 726.241	−5118.489
ρ	−2623.558	−177.11	3744.420	824.119	5003.927	2443.831

IV. DISCUSSION

A. Dispersion curves

As can be seen in Figs. 2–7, the calculated phonon-dispersion curves are nearly always within experimental uncertainty. In Ni and Cu, the biggest errors occur for the longitudinal branch at the zone edge for the [111] direction. For Pd, Pt, and Au, the biggest error is for the transverse branch at the same point. All together, these results provide strong support for the IEM.

The more traditional lattice dynamics calculations considering only ion-ion interactions require long-range interactions (out to five or ten neighbors) for similar quality fits, leading to computational complications and a lack of clear physical meaning in the parameters (they do not change smoothly as one goes down or across the Periodic Table). Thus in such models it is not clear what to do at a surface or defect or for an alloy. The IEM suggests that these long-range ion-ion interactions are equivalent to short-range terms involving electrons (many-body interactions). One approach that has been used to improve pairwise ion-ion methods is to add explicit volume-dependent terms.[11] However, this still leads to the compressibility paradox where the calculated compressibility in the long-wave limit is different from that found by the method of homogeneous deformation.[12]

An alternative approach of including many-body effects is the embedded atom method.[13] In this approach, the volume-dependent term is replaced by an electron density-dependent term that is usually expressed as a function of ion coordinates. The calculated phonon-dispersion relations by the embedded atom method for Cu, Pd, and Ni are in good agreement with experiments.[14,15]

Pseudopotential calculations[16–18] incorporating only two- and three-body interactions lead to phonon-dispersion relations similar to the IEM results, suggesting that both include the important many-body effects.

B. Parameters

The derivatives of the potential (ϕ' and ϕ'') show somewhat similar trends for the six metals considered here. Thus in all cases $\phi'_{i\text{-}i}$ is negative (repulsive) while $\phi'_{i\text{-}e}$ is positive (attractive). In addition, $\phi'_{i\text{-}i}$ is always less repulsive for the group-11 elements than for the group-10 elements. Similarly, $\phi'_{i\text{-}e}$ is always less attractive for group 11 compared with group 10. The magnitude of $\phi'_{i\text{-}i}$ and $\phi'_{i\text{-}e}$ also decreases going down the column of the Periodic Table for all cases except $\phi'_{i\text{-}e}$ of Au. The magnitude of $\phi'_{e\text{-}e}$ is always much smaller than either $\phi'_{i\text{-}e}$ or $\phi'_{i\text{-}i}$ but fluctuates a bit more. Thus $\phi'_{e\text{-}e}$ is attractive for Ni and Cu, repulsive for Pd, Pt, Ag, and Au, but nearly zero (slightly repulsive) for Cu.

The magnitudes for $\phi''_{i\text{-}e}$ and $\phi''_{e\text{-}e}$ are always positive, while $\phi''_{i\text{-}i}$ is positive for Ni and Cu but negative for Pd, Ag, Pt, and Au. $\phi''_{i\text{-}e}$ and $\phi''_{e\text{-}e}$ always decreasing going from group 10 to group 11. $\phi''_{i\text{-}e}$ and $\phi''_{e\text{-}e}$ increase going down a column except for $\phi''_{e\text{-}e}$ of Pd. There are somewhat more fluctuations in $\phi''_{i\text{-}i}$.

These close comparisons for parameters as a function of row and column of the Periodic Table suggest that $\phi(R)$ functions might be of general utility.

It is, of course, a serious approximation to include only nearest-neighbor interactions as done here. This approximation is equivalent to forcing $\phi(R)$ to zero between the first and second neighbors of each type and necessarily affects the values of the nearest-neighbor parameters differently. A better approximation would be to use the long-range potentials as discussed below.

C. Extensions

The next step in developing the IEM model is to relax the nearest-neighbor restriction by using longer-range functions such as

TABLE III. Force parameters for the IEM. All ϕ' are in units of dyn/10^8 and all ϕ'' are in units of dyn/cm=erg/cm^2.

	Ni	Cu	Pd	Ag	Pt	Au
$\phi'_{i\text{-}i}$	−27 704.468	−17 306.042	−24 577.434	−16 122.353	−18 844.026	−16 642.463
$\phi'_{i\text{-}e}$	29 927.634	20 918.248	36 409.394	21 203.767	31 581.288	24 698.151
$\phi'_{e\text{-}e}$	4622.578	320.127	−7284.208	−1683.551	−9817.455	−4982.972
$\phi''_{i\text{-}i}$	11 458.838	3416.790	−6398.258	−2407.357	−8582.474	−8841.528
$\phi''_{i\text{-}e}$	63 035.121	63 911.978	120 639.780	64 466.084	168 813.688	118 568.100
$\phi''_{e\text{-}e}$	9095.409	3578.843	5609.548	3840.405	14 726.241	5118.489

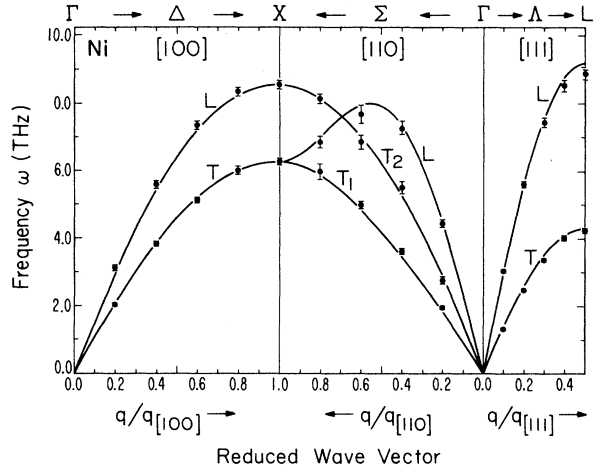

FIG. 2. Phonon dispersion for Ni: Dots represent experimental data (from Ref. 10). Solid lines are from the nearest-neighbor IEM.

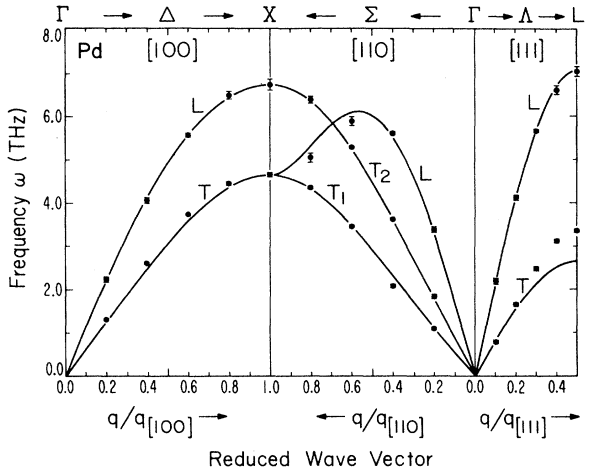

FIG. 4. Phonon dispersion for Pd: Dots represent experimental data (from Ref. 6). Solid lines are from the nearest-neighbor IEM.

$$\phi(R)=AR^{n}e^{-BR}(1+CR+\cdots) \tag{15}$$

and to fit the parameters $A,B,C,\ldots$ to the elastic constants and phonon curves. Using a superposition of such functions to describe the energy of the system in terms of ion and electron positions, we could allow the lattice to distort farther from equilibrium and calculate the energy and structure for a number of defects including stacking faults, vacancies, dislocations, surfaces, and grain boundaries. In such calculations the IEM electrons would not necessarily remain at the center of the tetrahedron and their location would be recalculated as a function of ion position (this is equivalent to the Born-Oppenheimer approximation). We intend to explore this in future work.

Since the electrons and nuclei can respond separately to external electric and magnetic fields, it will be interesting to examine transport properties (electrical and thermogalvanic). Allowing a finite mass for the electrons would make the Born-Oppenheimer breakdown important for electron transport in metallic systems. The magnitude of the electron mass could be determined by predicting the plasma oscillators and comparing with experiment.

For alloys and intermetallic compounds, we would expect the *e-i* and *e-e* terms to depend only on the number of nearest-neighbor ions of each type and to change smoothly as a function of composition. The *i-i* and *i-e* terms should depend on which ion is present and change smoothly after obtaining the full function of R for the various $\phi(R)$. We intend to examine some ordered phases (e.g., CuAu) to explore transferrability of the potentials.

This IEM approach is equally valid for hexagonal closest packed (hcp) systems; however, for hcp there are

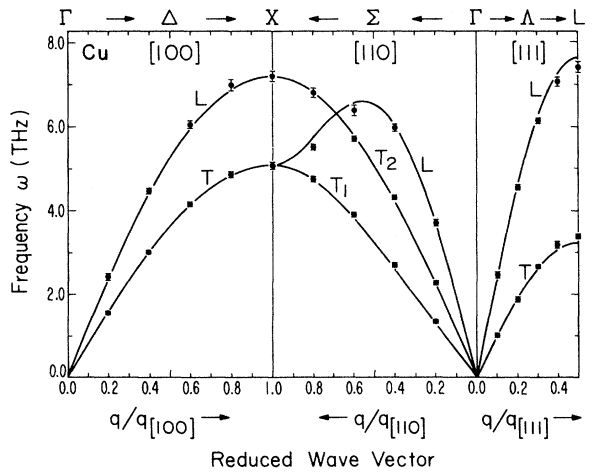

FIG. 3. Phonon dispersion for Cu: Dots represent experimental data (from Ref. 6). Solid lines are from the nearest-neighbor IEM.

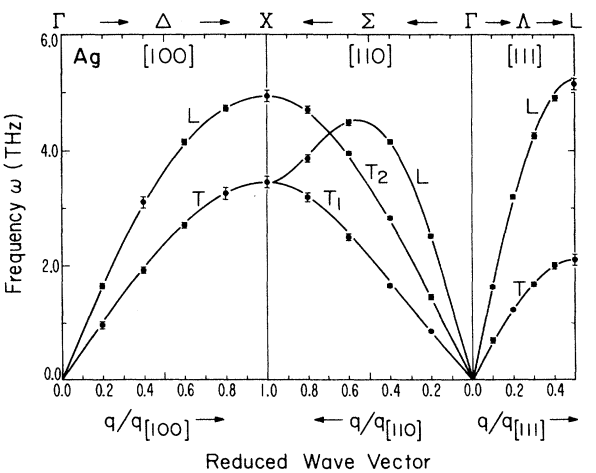

FIG. 5. Phonon dispersion for Ag: Dots represent experimental data (from Ref. 8). Solid lines are from the nearest-neighbor IEM.

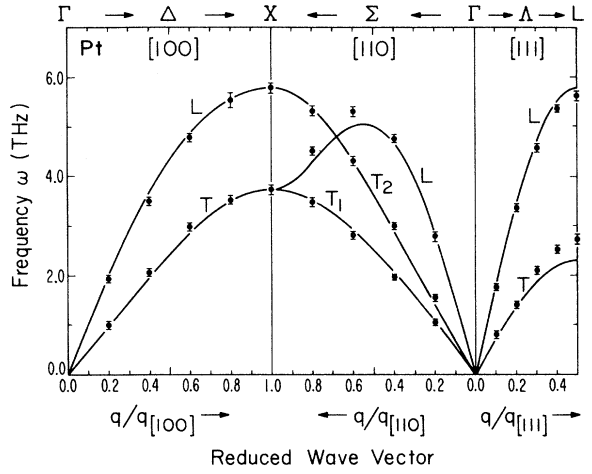

FIG. 6. Phonon dispersion for Pt: Dots represent experimental data (from Ref. 9). Solid lines are from the nearest-neighbor IEM.

two quite distinct *e-e* terms. There is a short-range interaction between tetrahedra that share faces (not present in fcc) and a long-range interaction between tetrahedra sharing corners. In contrast, the fcc system has tetrahedra sharing edges, leading to intermediate distances. To obtain the most accurate potentials, particularly $\phi_{e\text{-}e}(R)$, it would be useful to consider metals exhibiting both structures (fcc and hcp) fitting the potentials to relative energies in addition to elastic constants and phonon states. Although there are no experimental data for such systems, we could use the calculated properties from bulk band calculations as the input data to the IEM.

The concept of the IEM is based on calculations of clusters of Ni, Cu, Ag, Au, Li, and Na, where there is effectively only one valence electron (with a d^9 localized configuration on each Ni and a d^{10} configuration for the noble metals). Since there are two tetrahedral sites per atom in a fcc crystal, we consider that there is one-half an electron at each interstitial site. Thus in IEM, the *d* electrons (d^9 for group 10, d^{10} for group 11) are included in the ion terms. This is roughly equivalent to assuming that each atom has $n-1$ electrons in localized (small dispersion) band states and one electron in a delocalized (large dispersion) *sp* bond. This approximation is, we believe, most justified for group 11 and for the first transition row.

The GVB calculations on clusters suggest that as the number of electrons per tetrahedron (n_t) are increased from $\frac{1}{2}$ to 1 there is a tendency to stabilize the geometries with face-shared tetrahedra (hcp) but that for $n_t > 1$, the face-shared tetrahedra are strongly destabilized. Similarly, these calculations suggest that for edge-shared tetrahedra (fcc), $n_t > \frac{3}{2}$ is strongly destabilizing. It will be interesting to see if trends in $\phi_{e\text{-}e}$ bear out these expectations.

The assumption that the interstitial electrons localize in tetrahedra locations is based on the GVB calculations. These calculations do not suggest how much worse it will be to localize the electrons in octahedral sites nor have GVB calculations been carried out for bcc clusters to examine the character of the interstitial electrons. It would be interesting to make similar fits to these systems in order to obtain empirical data that might be useful in assessing the validity of these schemes.

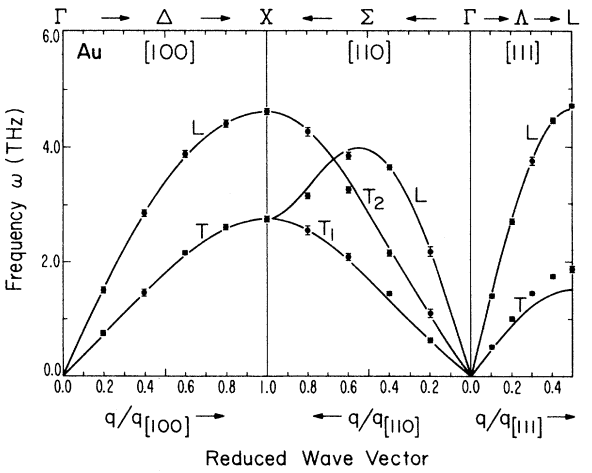

FIG. 7. Phonon dispersion for Au: Dots represent experimental data (from Ref. 7).

V. CONCLUSIONS

Treating the interstitial valence electrons as lattice particles and assuming that all interactions are pairwise and short ranged (only to first nearest neighbors), the IEM for lattice dynamics in fcc metals give quite satisfactory results for the phonon-dispersion relations at all **q** vectors for all the branches in the three symmetric directions with only six adjustable parameters. Since the parameters are directly related to the curvature and slope of the interparticle potentials at a particular position, they have a clear physical meaning that should be useful for describing distorted systems, surface reconstruction, etc. The inclusion of electrons in the force fields introduces no special computational complications and is simpler, for example, than using empirical pair interatomic interactions with crystal volume-dependent many-body contributions. Thus we believe that the IEM provides an attractive approach for developing force fields useful for calculating the structures and dynamics of metallic systems.

ACKNOWLEDGMENTS

This work was initiated with support from the National Science Foundation—Materials Research Groups

(Grant No. DMR-8811795) and completed with support from the Air Force Office of Scientific Research (Grant No. AFOSR-88-0051). One of the authors (M.L.) would like to thank Dr. Channing Ahn for assisting him in the use of the Caltech Materials Research Group computer facilities.

APPENDIX

Using two-body interactions for each pair of lattice particles (ion-ion, ion-electron, electron-ion, and electron-electron) leads to force constant matrices of the form

$$\Phi_{\alpha\beta}\begin{bmatrix} l & l' \\ k & k' \end{bmatrix} = \phi'\begin{bmatrix} l & l' \\ k & k' \end{bmatrix}\left[\frac{x_\alpha\begin{bmatrix} l & l' \\ k & k' \end{bmatrix}x_\beta\begin{bmatrix} l & l' \\ k & k' \end{bmatrix}}{r^3\begin{bmatrix} l & l' \\ k & k' \end{bmatrix}} - \frac{\delta_{\alpha\beta}}{r^2\begin{bmatrix} l & l' \\ k & k' \end{bmatrix}}\right] - \phi''\begin{bmatrix} l & l' \\ k & k' \end{bmatrix}\frac{x_\alpha\begin{bmatrix} l & l' \\ k & k' \end{bmatrix}x_\beta\begin{bmatrix} l & l' \\ k & k' \end{bmatrix}}{r^2\begin{bmatrix} l & l' \\ k & k' \end{bmatrix}} \tag{A1}$$

where only two parameters ϕ' and ϕ'', are required to describe the interactions of nearest neighbors.

The number of components of the force constant matrices can be further reduced by using the space group symmetry of the crystal for unit cell containing one ion and two electrons. For nearest-neighbors interactions this leads to a total of seven force constant matrix components. For instance, the interaction between the electron at $[\frac{\bar{1}}{4}\frac{\bar{1}}{4}\frac{\bar{1}}{4}]$ and the ion at [000] is

$$\Phi_{\alpha\beta}\begin{bmatrix} l & l' \\ 2 & 0 \end{bmatrix}_{e\text{-}i} = \begin{bmatrix} \mu & \lambda & \lambda \\ \lambda & \mu & \lambda \\ \lambda & \lambda & \mu \end{bmatrix} \tag{A2}$$

where $\mu=\Phi_{11}(\begin{smallmatrix} l & l' \\ 2 & 0 \end{smallmatrix})_{e\text{-}i}$, $\lambda=\Phi_{12}(\begin{smallmatrix} l & l' \\ 2 & 0 \end{smallmatrix})_{e\text{-}i}$, and where the ion and two electrons of the unit cell are denoted 0, 1, and 2, respectively.

The interaction between the electron at $[\frac{1}{4}\frac{1}{4}\frac{1}{4}]$ and the ion at [000] gives the force constant matrix

$$\Phi_{\alpha\beta}\begin{bmatrix} l & l' \\ 1 & 0 \end{bmatrix}_{e\text{-}i} = \begin{bmatrix} \mu & \bar{\lambda} & \bar{\lambda} \\ \bar{\lambda} & \mu & \lambda \\ \bar{\lambda} & \lambda & \mu \end{bmatrix}. \tag{A3}$$

For ions sitting in positions different from [000], the corresponding force constant matrices of the electron-ion interaction are obtained through the operations of tetrahedral symmetry. The $\Phi_{i\text{-}e}$ between a [000] ion and a $[\frac{1}{4}\frac{1}{4}\frac{1}{4}]$ electron is given by (A2) and that between a [000] ion and a $[\frac{\bar{1}}{4}\frac{\bar{1}}{4}\frac{\bar{1}}{4}]$ electron is given by (A3).

The symmetry group for the ion-ion and electron-electron interactions is simple, and the corresponding force constant matrices are also given herein. For ions located at [000] and $[\frac{1}{2},\frac{1}{2},0]$, we obtain

$$\Phi_{\alpha\beta}\begin{bmatrix} l & l' \\ 0 & 0 \end{bmatrix}_{i\text{-}i} = \begin{bmatrix} \alpha & \gamma & 0 \\ \gamma & \alpha & 0 \\ 0 & 0 & \beta \end{bmatrix} \tag{A4}$$

where $\alpha=\Phi_{11}(\begin{smallmatrix} l & l' \\ 0 & 0 \end{smallmatrix})_{i\text{-}i}$ and $\gamma=\Phi_{12}(\begin{smallmatrix} l & l' \\ 0 & 0 \end{smallmatrix})_{i\text{-}i}$, and $B=\Phi_{33}(\begin{smallmatrix} ll' \\ 00 \end{smallmatrix})_{i\text{-}i}$. For pair interactions, we have $B=\alpha-\gamma$. For electrons sitting at $[\frac{3}{4}\frac{1}{4}\frac{1}{4}]$ and $[\frac{1}{4}\frac{1}{4}\frac{1}{4}]$, we obtain

$$\Phi_{\alpha\beta}\begin{bmatrix} l & l' \\ 1 & 2 \end{bmatrix}_{e\text{-}e} = \begin{bmatrix} \delta & 0 & 0 \\ 0 & \rho & 0 \\ 0 & 0 & \rho \end{bmatrix} \tag{A5}$$

where $\delta=\Phi_{11}(\begin{smallmatrix} l & l' \\ 1 & 2 \end{smallmatrix})_{e\text{-}e}$ and $\rho=\Phi_{22}(\begin{smallmatrix} l & l' \\ 1 & 2 \end{smallmatrix})_{e\text{-}e}$.

The phonon-dispersion relations in the [110] direction are given by

$$+\frac{8\left[\mu\cos^2\left[\frac{\pi}{2}q\right]-\lambda\sin^2\left[\frac{\pi}{2}q\right]\right]^2}{(\delta+\rho)\sin^2\left[\frac{\pi}{2}q\right]+\mu}+\frac{4\lambda^2\sin^2(\pi q)}{2\rho\cos^2\left[\frac{\pi}{2}q\right]+(\delta+\mu)}, \tag{A6}$$

$$M_k\omega^2_{T_2}(\mathbf{q})=-4(\alpha-\gamma)\sin^2(\pi q)-16\alpha\sin^2\left[\frac{\pi}{2}q\right]-8\mu+\frac{8\mu^2\cos^4\left[\frac{\pi}{2}q\right]}{2\rho\sin^2\left[\frac{\pi}{2}q\right]+\mu}+\frac{4\lambda^2\sin^2(\pi q)}{(\delta+\rho)\cos^2(\pi q)+(\mu+\rho)}, \tag{A7}$$

$$M_k\omega_L^2(\mathbf{q})=-4(\alpha-\gamma)\sin^2(\pi q)-8(2\alpha-\gamma)\sin^2\left[\frac{\pi}{2}q\right]-8\mu+\frac{8\left[\mu\cos^2\left[\frac{\pi}{2}q\right]+\lambda\sin^2\left[\frac{\pi}{2}q\right]\right]^2}{(\delta+\rho)\sin^2\left[\frac{\pi}{2}q\right]+\mu}, \tag{A8}$$

where T_1 is polarized in the $[1\bar{1}0]$ direction and T_2 is polarized in the [001] direction. The [111] branches are given as follows:

$$M_k\omega_T^2(\mathbf{q})=-4(3\alpha-2\gamma)\sin^2(\pi q)-8\mu$$
$$+\frac{\left[(\mu-\lambda)\cos\left[\frac{3\pi}{2}q\right]+(3\mu+\lambda)\cos\left[\frac{\pi}{2}q\right]\right]^2}{2\left[2\rho\sin^2\left[\frac{\pi}{2}q\right]+\mu\right]}$$
$$+\frac{\left[(\mu-\lambda)\sin\left[\frac{3\pi}{2}q\right]-(3\mu+\lambda)\sin\left[\frac{\pi}{2}q\right]\right]^2}{2\left[2\rho\cos^2\left[\frac{\pi}{2}q\right]+\mu+\delta\right]}, \tag{A9}$$

$$M_k\omega_L^2(\mathbf{q})=-4(3\alpha+\gamma)\sin^2(\pi q)-8\mu$$
$$+\frac{\left[(\mu+2\lambda^2)\cos\left[\frac{3\pi}{2}q\right]+(3\mu-2\lambda)\cos\left[\frac{\pi}{2}q\right]\right]^2}{2\left[2\rho\sin^2\left[\frac{\pi}{2}q\right]+\mu\right]}$$
$$+\frac{\left[(\mu+2\lambda)\sin\left[\frac{3\pi}{2}q\right]+(3\mu-2\lambda)\sin\left[\frac{\pi}{2}q\right]\right]^2}{2\left[2\rho\cos^2\left[\frac{\pi}{2}q\right]+\mu+\delta\right]}. \tag{A10}$$

[1]M. H. McAdon and W. A. Goddard III, J. Phys. Chem. **91**, 2607 (1987).

[2]M. H. McAdon and W. A. Goddard III, Phys. Rev. Lett. **55**, 2563 (1985).

[3]H. B. Huntington, *Solid State Physics,* edited by F. Seitz and D. Turnbull (Academic, New York, 1958), Vol. 7, p. 214.

[4]R. O. Simmons and H. Wang, *Wingle Crystal Elastic Constants and Calculated Aggregate Properties: A Handbook* (MIT Press, Cambridge, 1971).

[5]W. B. Pearson, *Handbook of Lattice Spacings and Structures of Metals and Alloys* (Pergamon, Oxford, 1967).

[6]A. P. Miller and B. N. Brockhouse, Can. J. Phys. **49**, 704 (1971); E. C. Svensson, B. Brockhouse, and J. M. Rowe, Phys. Rev. **155**, 619 (1967).

[7]J. W. Lynn, H. G. Smith, and R. M. Nicklow, Phys. Rev. B **8**, 3493 (1973).

[8]W. A. Kamitakahara and B. N. Brockhouse, Phys. Lett. **29A**, 639 (1969).

[9]R. Ohrlich and W. Drexel, in *4th IAEA Symposium on Inelastic Scattering of Neutrons* (IAEA, Vienna, 1968), Vol. 1, p. 203.

[10]R. J. Birgeneau, J. Cordes, G. Dolling, and A. D. B. Woods, Phys. Rev. A **136**, 1359 (1964).

[11]R. A. Johnson, Phys. Rev. B **6**, 2094 (1972).

[12]D. C. Wallace, Phys. Rev. **182**, 778 (1969).

[13]M. S. Daw and M. I. Baskes, Phys. Rev. B **29**, 6443 (1984).

[14]J. S. Nelson, E. C. Sowa, and M. S. Daw, Phys. Rev. Lett. **61**, 1977 (1988).
[15]M. S. Daw and R. D. Hatcher, Solid State Commun. **56**, 697 (1985).
[16]A. O. Animalu, Phys. Rev. B **8**, 3542 (1973).
[17]A. O. Animalu, Phys. Rev. B **8**, 3555 (1973).
[18]D. Prakash and J. C. Upadhyaya, J. Phys. Chem. Solids **49**, 91 (1988).